JOINT EUROPEAN TORUS

JET–P(88)60

A. Gondhalekar, A.D. Cheetham, J.C.M de Haas, O.N. Jarvis, P.D. Morgan,
J. O'Rourke, G. Sadler and M.L. Watkins

Correlation of Heat and Particle Transport in JET

Correlation of Heat and Particle Transport in JET

A. Gondhalekar, A.D. Cheetham, J.C.M de Haas[1], O.N. Jarvis, P.D. Morgan, J. O'Rourke, G. Sadler and M.L. Watkins

JET-Joint Undertaking, Culham Science Centre, OX14 3DB, Abingdon, UK

[1]FOM Instituut voor Plasmafysica "Rijnhuizen", The Netherlands

Preprint of Paper to be submitted for publication in the Proceedings of
IAEA Technical Committee Meeting on Pellet Injection and Toroidal Confinement,
Gut Ising, West Germany, 24th-26th October 1988

Submitted for publication in Proceedings of IAEA Technical Committee Meeting on Pellet Injection and Toroidal Confinement, Gut Ising, W. Germany, 24th-26th October 1988.

CORRELATION OF HEAT AND PARTICLE TRANSPORT IN JET

A Gondhalekar, A D Cheetham, J C M de Haas*, O N Jarvis, P D Morgan, J O'Rourke, G Sadler and M L Watkins.

JET Joint Undertaking, Abingdon, OX14 3EA, UK.
*FOM Instituut voor Plasmafysica "Rijnhuizen", The Netherlands.

ABSTRACT

Radial thermal and particle diffusivities have been measured using transient methods, yielding χ and D simultaneously in the plasma interior at $0.5 \leq r/a \leq 0.7$. $\chi_e = 2.7 \pm 0.4$ m^2/s and $D_e = 0.4 \pm 0.1$ m^2/s have been measured in OH plasmas, giving $\chi_e/D_e = 6.8 \pm 2.7$. NBI heated H-mode plasmas are indistinguishable from OH plasmas in respect of χ_e, D_e and χ_e/D_e. The ion thermal diffusivity has also been measured in H-mode plasmas, giving $1 < \chi_i(m^2/s) < 3$, simultaneously with $\chi_e = 3 \pm 0.5$ m^2/s, thus $0.3 < \chi_i/\chi_e < 1$. The large value of χ_e/D_e would suggest that micro-magnetic stochasticity, rather than $\underline{E} \times \underline{B}$ convection, may be the key mechanism in anomalous transport.

1. INTRODUCTION

An important objective in tokamak research is to find suitable descriptions for the measured radial thermal and particle fluxes, and to identify the underlying mechanism of transport. Many models for transport in tokamaks have been developed which make specific predictions for correlations between thermal and particle transport[1]. Correlations amongst the transport coefficients arise due to mutual interference between the simultaneously occuring processes in the system, which are described by some form of Onsager relations. In order to exclude some of the contending models, accurate measurements of the correlations are required. To reduce uncertainties arising from shot-to-shot and spatial variations it is necessary to determine these coefficients simultaneously in the same spatial region of the plasma. We expect that static experiments involving steady-state analysis for the determination of correlations between transport coefficients will be inconclusive, and that transient methods which do not strongly perturb the plasma are more appropriate.

We present simultaneous measurements of radial thermal and particle transport coefficients by analysis of inward propagation of temperature and density perturbations produced when a small pellet is injected into the plasma. The results are compared with those from other transient techniques (a) measurements of the velocity and damping of electron temperature and density pulses propagating outwards following a sawtooth collapse, (b) time dependent transport analysis applied to non-stationary plasmas. This paper incorporates results from earlier publications[2], where details of the applied methods are given. Other transient methods to measure electron density and thermal transport, by modulating the sources, have been applied in JET[3,4]. However those methods cannot be applied simultaneously.

In the following we contrast thermal and particle transport behaviour in Ohmically heated(OH) deuterium plasmas in the outer-limiter configuration in the parameter range I_ϕ=3MA, $2.8 \leq B_\phi(T) \leq 3.4$, $T_e(0) \cong 3$ keV, $T_i(0) \cong 1.5$ keV and $1.5 \leq \bar{n}_e(10^{19} m^{-3}) \leq 2.7$, with that in H-mode deuterium plasmas limited by a magnetic separatrix formed during single-null x-point operation, in the parameter range I_ϕ=3MA, $B_\phi \approx 3$T, $T_e(0) \approx T_i(0) \approx 5$keV, $\bar{n}_e \cong 5 \times 10^{19}$ m^{-3}, and $\cong 8$ MW of NBI heating, in the same spatial region. Table I summarizes the measurements.

2. DETERMINATION OF χ_e, D_e, AND χ_i BY PELLET INJECTION

Local thermal and particle diffusivities are determined by analysis of propagation of perturbations of temperature and density. The perturbation is caused by a small pellet injected in the horizontal mid-plane, penetrating to a radius r_p such that $r_p/a \approx 0.7$, where a is the minor radius. The propagation is analyzed in the region $r_c < r < r_p$, where r_c is the sawtooth inversion radius. Typically, in the investigations reported here, $0.3 \leq r_c/a \leq 0.5$ for the OH and $r_c/a \approx 0.35$ for the H-mode cases. In previous investigations [5,6] we have shown that the radial propagation of electron temperature and density perturbations caused by pellet injection may be representative of the local transport properties of the target plasma in the region $r_c < r < r_p$.

2.1 ELECTRON THERMAL DIFFUSIVITY

χ_e is determined by comparing the measured temporal evolution of $T_e(r)$ in the region $r_c < r < r_p$ with a simulation using a diffusive model including sources,

$$(3/2)n_e(r)d(kT_e(r))/dt = -\mathrm{div}Q_e + S(r) \qquad -1-$$

where $Q_e = -\chi_e(r)n_e(r)\nabla(kT_e(r))$, $S(r)$ the thermal source, and k is the Boltzmann constant. A convective term in the expression for Q_e is suggested by steady-state power balance analysis[7], but is ignored here; a negative flux term(pinch) will increase the inferred χ_e, and a positive flux will decrease it. The initial condition for solving eq.1, $T_e(r,t=0)$ and $n_e(r,t=0)$, the temperature and density profiles instantly after pellet injection, are determined from measurements of $T_e(r)$, $n_e(r)$, pellet mass, ablation rate and penetration depth. Fig.1 shows $T_e(r)$ and $n_e(r)$ immediately before and after pellet injection. The pellet deposition profile is calculated using the neutral gas and plasma shielding model of pellet ablation[8,9]. The model reproduces both the pellet penetration, as seen by the soft x-ray cameras viewing the pellet trajectory, and the maximum in the density deposition, as seen in the measurement of $n_e(r)$. During evolution of $T_e(r)$ the perturbed density profile is assumed to be stationary. This is justified because the density perturbation travels much more slowly than the temperature perturbation, as will become clear in the following. $S(r)$ is calculated for the equilibrium pre-pellet plasma, and is assumed to remain stationary thereafter; the pellet injection events analyzed are such that perturbations in total heating power and in radiation and charge-exchange losses may be neglected. The modelled evolution of $T_e(r)$ is found to be sensitive only to the local value of χ_e, which is iterated until good agreement with the measured $T_e(r,t)$ is obtained. Fig.2 shows a representative comparison between measured and modelled $T_e(r,t)$ at four radii. $\chi_e = 2.8 \pm 0.3$ m^2/s for the OH plasmas, and $\chi_e = 3 \pm 0.5$ m^2/s for the H-mode plasmas are obtained.

2.2 ELECTRON PARTICLE DIFFUSIVITY

D_e is determined analogously by comparing the temporal evolution of $n_e(r)$ with a simulation using a diffusive model including sources.

$$dn_e(r)/dt = -div\Gamma_e(r) + S_e(r) \qquad -2-$$

where $\Gamma_e(r) = -D_e(r)\nabla n_e(r) + \Gamma_p(r)$, and $S_e(r)$ is the electron source. The diffusion coefficient is represented as $D_e(r)=D_0(1+2r^2/a^2)$ and the pinching flux $\Gamma_p(r)=n_e(r)V_p(r)$. This form for $D_e(r)$ is justified by our previous measurements of density profile dynamics in JET [3,8,10]. $D_e(r)$ is specified for the equilibrium $n_e(r)$ and with the appropriate total $S_e(r)$, the pinch velocity $V_p(r)$ is self-consistently calculated. With these values of $D_e(r)$, $S_e(r)$ and $V_p(r)$ the temporal evolution of $n_e(r)$ is calculated. D_0 is iterated until a match with the measured $n_e(r,t)$ is achieved. For the OH plasmas $D_e=0.4\pm0.1$ m^2/s, and for the H-mode plasmas $D_e=0.3$-0.6 m^2/s. The large uncertainty in D_e for the H-mode arises due to uncertainties in determining the particle source.

2.3 ION THERMAL DIFFUSIVITY

χ_i is similarly determined by analyzing propagation of an ion temperature perturbation. Since the ion temperature cannot at present be measured with the required spatial and temporal resolution, we have employed propagation of perturbations of thermonuclear neutron emission, as evidenced by a multi-chord neutron camera, viewing a poloidal cross-section of the plasma from above, to deduce χ_i. In OH plasmas T_i is not high enough to give sufficient neutron flux to the camera for high quality neutron emission profile analysis. Therefore only the NBI heated H-mode plasmas have been analyzed for the χ_i determination. Fig.3 shows the temporal evolution of line-integrated neutron emission in five of the chords viewing the outside half of the plasma cross-section. The pellet is injected at t=54.8s, which reduces T_i for $r \geq r_p$. Fig.3 shows that the neutron emission on the chord passing through the cold plasma(‡‡ 19) also instantaneously drops, whereas the neutron emission on the chords viewing the plasma further inside drops more slowly. In fig.3 we observe a neutron emissivity perturbation due to an ion temperature 'cold' front travelling diffusively into the plasma. We have modelled this process as follows. The equilibrium (pre-pellet) deuteron density profile, $n_i(r)$, is constructed from the measured profiles $n_e(r)$ and $Z_{eff}(r)$. The pre-pellet deuteron temperature profile, $T_i(r)$, is assumed to be Gaussian with the measured peak value $T_i(0)$. The width of the Gaussian is adjusted to match the thermonuclear part of the measured neutron yield, taking into account the proportion of beam-plasma and thermonuclear neutron yield which is deduced from a model calculation of neutral beam dynamics within the TRANSP code[11]. The model calculation also gives spatial emissivity profiles for neutrons from each of the two reactions.

After pellet injection the beam-plasma neutron emissivity profile is assumed to remain unchanged, which is reasonable since the pellet produces only a small perturbation of the plasma parameters, and the NBI power remains constant. The observed perturbations in the total neutron yield are attributed to perturbations of ion temperature and its consequences for the thermonuclear neutrons. The initial condition for solving the diffusion

equation for χ_i, analogous to eq.1, is the deuteron density and temperature profiles immediatly after pellet injection. $n_i(r,t=0)$ is deduced as in sec.2.1, and $T_i(r,t=0)$ is derived by assuming adiabatic response of the ion temperature. The temporal evolution of $T_i(r)$, the corresponding thermonuclear neutron emissivity, and the total line-integrated neutron emission observed in each cord of the neutron camera are calculated. The perturbed $n_i(r)$ is assumed to be stationary during evolution of $T_i(r)$. The value of χ_i in the measurement region is iterated until a match is obtained with the observed temporal evolution of the emission, fig.4. This procedure yields $1<\chi_i(m^2/s)<3$, simultaneously with $\chi_e=3\pm0.5$ m^2/s, giving $0.3<\chi_i/\chi_e<1$ for the H-mode plasma.

3. CONCLUSIONS

Table I summarizes the observations. Simultaneous direct measurements of thermal and particle transport yield $\chi_e=2.7\pm0.4$ m^2/s and $D_e=0.4\pm0.1$ m^2/s, giving $\chi_e/D_e=6.8\pm2.7$ at $0.5\leq r/a\leq0.7$ in the OH plasmas. The H-mode plasmas, with $\cong$8MW of NBI heating, are indistinguishable from the OH plasmas in respect of χ_e, D_e, and χ_e/D_e. The ion thermal diffusivity has also been determined in the specified region for the H-mode plasmas, giving $1<\chi_i(m^2/s)<3$, thus $0.3<\chi_i/\chi_e<1$. An aim of our future work is to incorporate impurity transport into this scheme.

The large value of χ_e/D_e would suggest that micro-magnetic stochasticity, rather than $\underline{E}x\underline{B}$ convection, may be the primary contributing mechanism in the observed anomalous transport. The above observations are contrary to those reported from other experiments[12,13], where thermal and particle diffusivities of equal magnitude are deduced. The measurements presented here appear to be consistent with expectations of the critical temperature gradient model of anamolous transport[14,15]. The simililarity of OH limiter plasmas and NBI heated H-mode plasmas in respect of the electron thermal and particle transport behaviour in the plasma interior suggests that the same underlying mechanism of anomalous transport is operative in the two cases, although they are quite different in respect of magnetic configuration, temperature range, and density profile shape. The intrinsically better particle (vs thermal) confinement witnessed here, which will similarly affect recycled impurities and helium ash, may pose the more severe barrier to future reactor-oriented tokamak experiments

ACKNOWLEDGEMENTS

The authors are grateful to J Fessey and D Garton for computational support, to J M Adams, M von Hellermann, D Muir, P D Larsen and N Watkins for providing and validating data.

Table I: Some Elements of the Transport Matrix

	OH plasma limiter plasma			
	$\chi_e(m^2/s)$	$D_e(m^2/s)$	$\Gamma_p(10^{18}/m^2.s)$	r/a
(a)	2.8± 0.3	0.4±0.1	2± 0.7	≈ 0.6
(b)	2.9± 0.4	0.4±0.2	-	≈ 0.7
(c)		0.5±0.1	1.5±0.2	≈ 0.7

	NBI heated H-mode plasma			
	$\chi_e(m^2/s)$	$D_e(m^2/s)$	$\chi_i(m^2/s)$	r/a
(a)	3±0.5	0.3-0.6	1-3	≈ 0.5
(b)	3±0.6	-	-	≈ 0.6
(c)	2(d)	0.2-0.3	-	≈ 0.5
		0.3-0.4	-	≈ 0.7

where
(a) Pellet Injection.
(b) Analysis of sawtooth density and heat pulse[2,16,17].
(c) Time dependent transport analysis, 'flux-gradient' method[2,7].
Thermal flux model $Q(r) = -\chi(r)n(r)\nabla T(r) + Q_p(r)$
Particle flux model $\Gamma_e(r) = -D_e(r)\nabla n_e(r) + \Gamma_p(r)$
Assumed $T(r) = T_e(r)$. Inferred χ is for a single fluid plasma.
(d) H-mode at I_ϕ = 2MA, B_ϕ = 2T, different from the other data

REFERENCES

[1] J D Callen, JET Report JET-IR(87)07.

[2] A Gondhalekar, et al., 15th Euro. Conf. on Controlled Fusion and Plasma Physics, Dubrovnik 1988. Europhys. Conf. Abstracts Vol 12b part I, p.151, and
A D Cheetham, et al., 12th IAEA Conf. on Plasma Physics and Controlled Nuclear Fusion Research, Nice 1988. Paper IAEA-CN-50/I-2-2.

[3] A Gondhalekar, et al., Bull. Am. Phys. Soc.30 (1985) 1525 and JET Report JET-P(85)31.

[4] D F H Start, et al., 12th IAEA Conf. on Plasma Physics and Controlled Nuclear Fusion Research, Nice 1988. Paper IAEA-CN-50/E-2-3.

[5] A D Cheetham, et al., 14th Euro. Conf. on Controlled Fusion and Plasma Physics, Madrid, 1987. Europhys. Conf. Abstracts Vol 11d, part I, p.205.

[6] A D Cheetham, et al., Proc. International School of Plasma Physics, Varenna 1986. CEC Publication EUR 10797 EN, vol.2, 681.

[7] J D Callen et al., Nuclear Fusion 27 (1987) 1857.

[8] A Gondhalekar, et al., 11th IAEA Conf on Plasma Physics and Controlled Nuclear Fusion Research, Kyoto 1986. Proceedings, Vol 3, p.457.

[9] M L Watkins, et at., 14th Euro. Conf. on Controlled Fusion and Plasma Physics, Madrid, 1987. Europhys. Conf. Abstracts Vol 11d, part I, p.201.

[10] A D Cheetham, et al., 13th Euro. Conf. on Controlled Fusion and Plasma Physics, Schliersee, 1986. Europhys Conf. Abstracts Vol 10c, part I, p.240.

[11] R J Goldston, et al., J.Comput. Physics 43(1981)61.

[12] S K Kim, et al., 15th Euro. Conf. on Controlled Fusion and Plasma Physics, Dubrovnik, 1988. Europhys. Conf. Abstracts Vol 12b, part I, p.187.

[13] P C Efthimion, et al., 12th IAEA Conf. on Plasma Physics and Controlled Nuclear Fusion Research, Nice 1988. Paper IAEA-CN-50/A-V-4.

[14] P H Rebut, et al., 11th IAEA Conf. on Plasma Physics and Controlled Nuclear Fusion Research, Kyoto 1986. Proceedings, 2(1987)187.

[15] P H Rebut, et al., 12th IAEA Conf. on Plasma Physics and Controlled Nuclear Fusion Research, Nice 1988. Paper IAEA-CN-50/D-4-1.

[16] A Hubbard, et al., 13th Euro. Conf. on Controlled Fusion and Plasma Physics, Schliersee 1986. Europhys. Conf. Abstracts Vol 10c, part I, p.232.

[17] B J D Tubbing, et al., Nuclear Fusion 27 (1987) 1843, and N J Lopes Cardozo, et al., Nuclear Fusion 28 (1988) 1173.

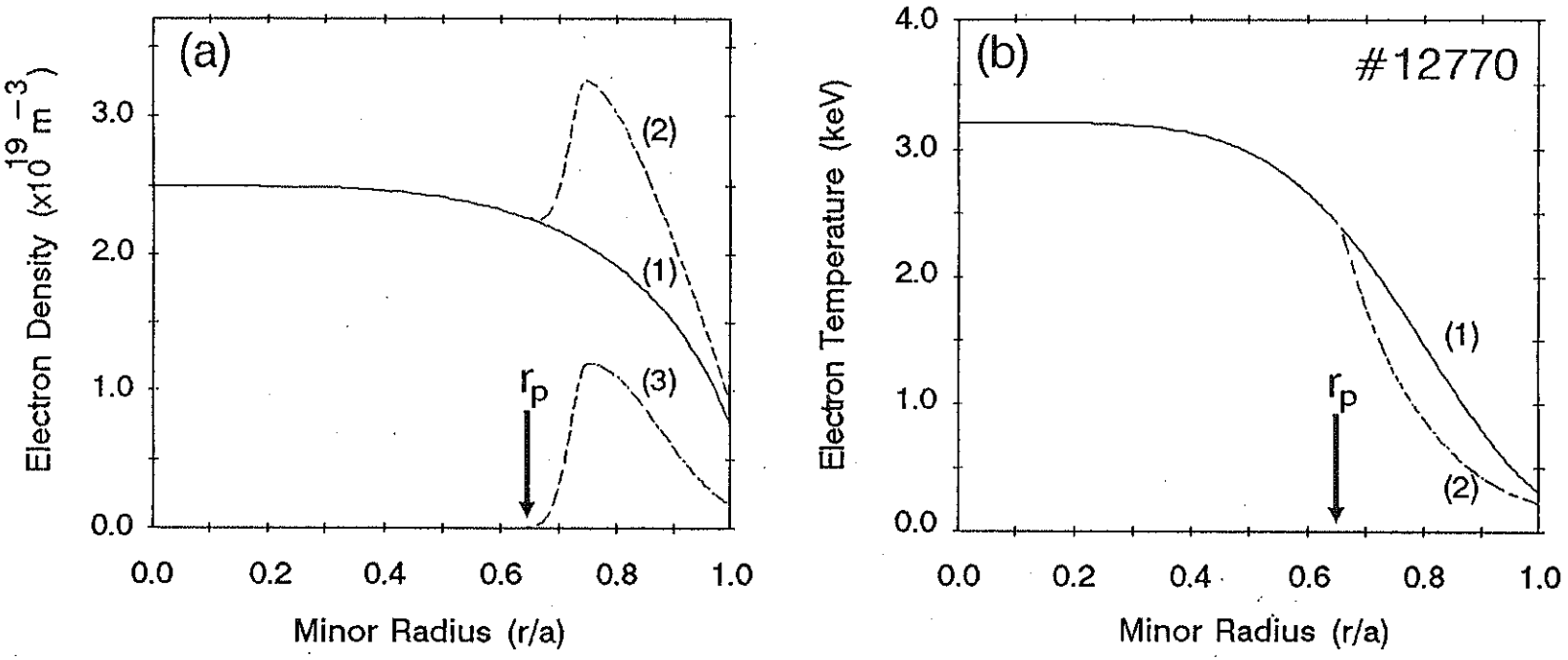

Figure 1: (a) Pre-pellet radial profile of the electron density(1) the pellet deposition profile (3); and the total post-pellet density profile (2).
(b) Pre-pellet radial electron temperature profile (1) and post-pellet Te profile (2).
The profiles (a2) and (b2) are the initial conditions for the transport calculation.

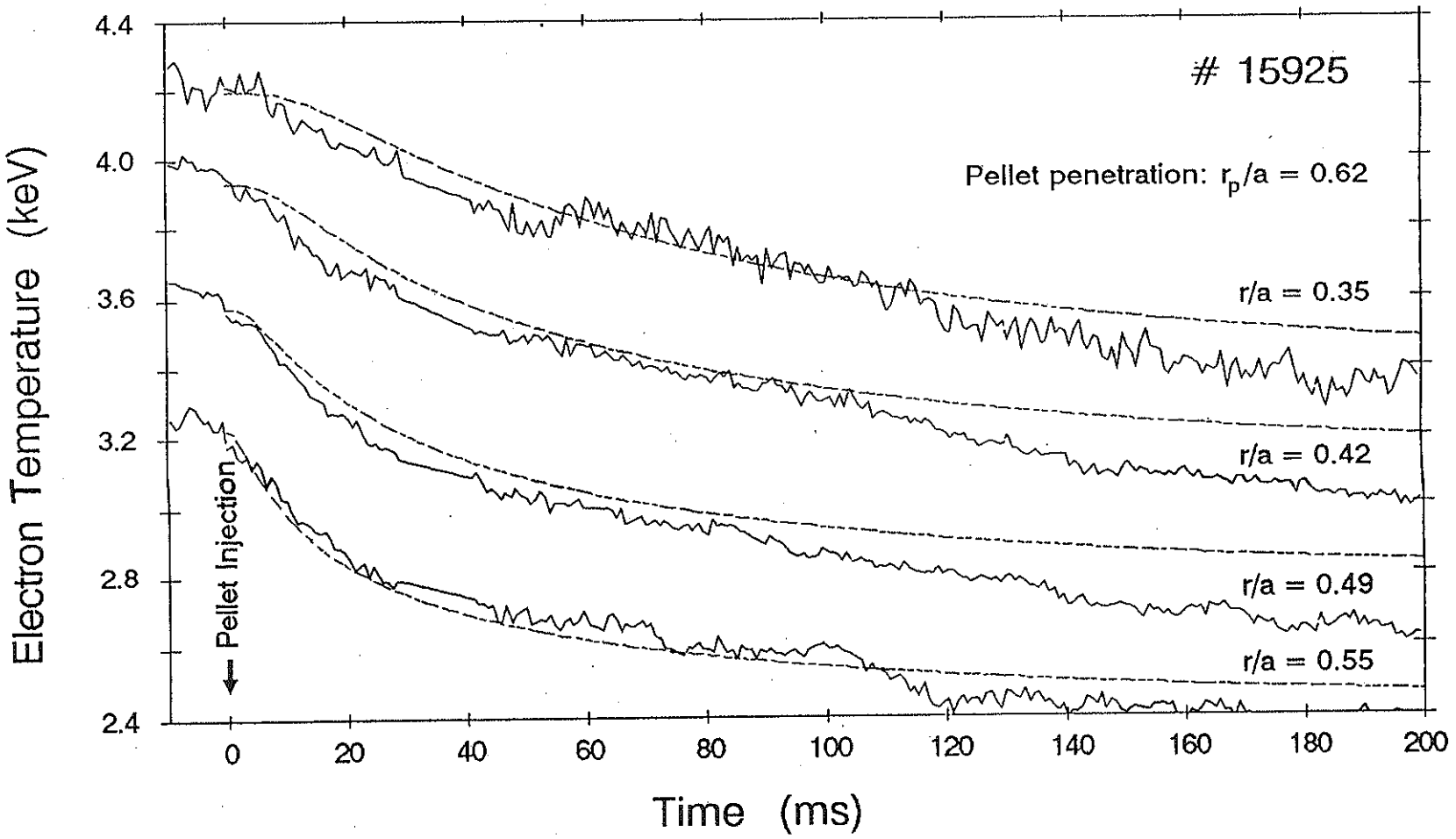

Figure 2: The temporal evolution of the electron temperature at different radii (r/a) after the injection of a pellet. The full line is the ECE temperature, and the dashed line is the modelled evolution.

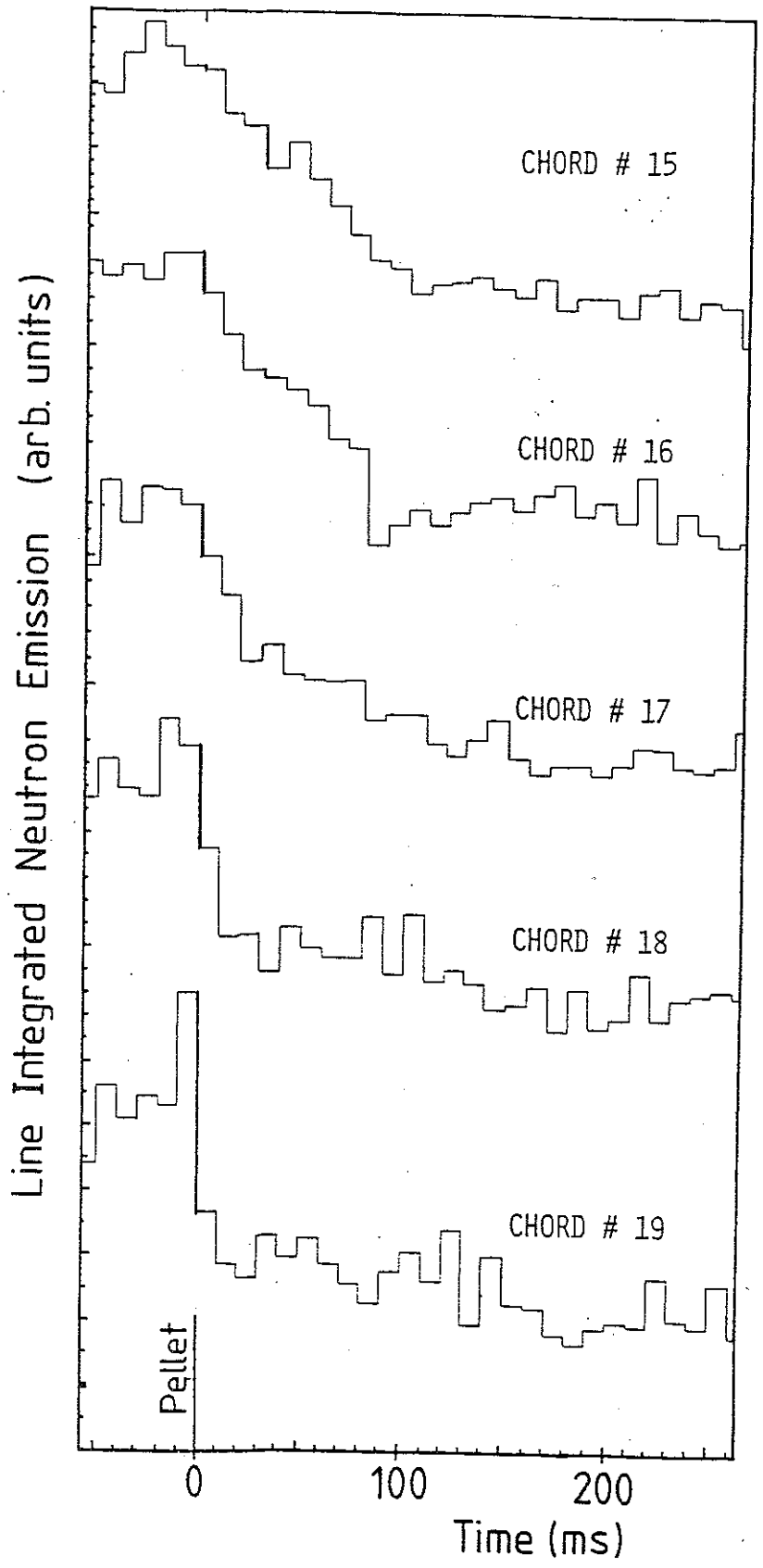

Figure 3: Evolution of line integrated neutron emission after pellet injection along chords with major radius between 3.78m(chord 19) and 3.02m(chord 15).

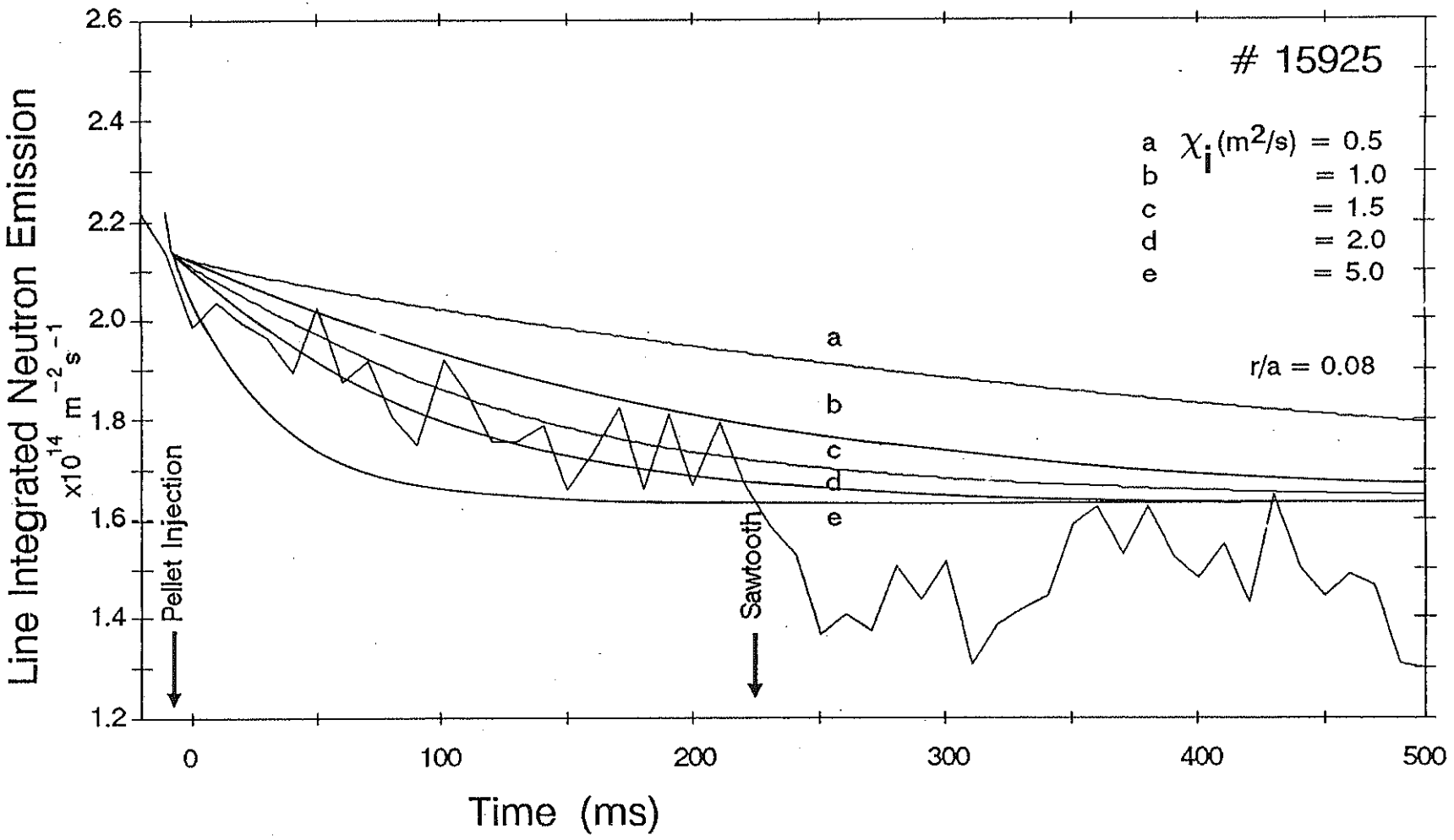

Figure 4: Comparison of modelled and measured temporal evolution of the line integrated neutron emission for different values of the assumed χ_i.